Available online at www.sciencedirect.com
SCIENCE DIRECT®
Journal of Solid State Chemistry 178 (2005) 2001–2007
JOURNAL OF SOLID STATE CHEMISTRY
www.elsevier.com/locate/jssc

Stabilized epitaxial films of hexagonal $Ni_{1-x}S$ on MgO(001)

Hiroshi Nozaki*, Takashi Aizawa, Kousuke Kosuda

National Institute for Materials Science, 1-1 Namiki, Tsukuba, Ibaraki, 305-0044, Japan

Received 14 February 2005; received in revised form 2 April 2005; accepted 7 April 2005
Available online 4 May 2005

Abstract

This study used molecular beam epitaxy to prepare epitaxial $Ni_{1-x}S$ films with NiAs-type structures on MgO(001) substrates. The films were characterized using X-ray diffraction method. Nickel vacancies showed an ordered arrangement of alternating metal-rich and metal-deficient layers along the *c*-axis. The orientations of epitaxial films were (001) [1,−1,0]$Ni_{1-x}S$||(001)[110]MgO and its equivalents because of the coexistence of the trigonal axis of the $Ni_{1-x}S$ film and the four-fold rotation axis of the MgO substrate. Film compositions were obtained using intensity ratios between 0 0 1 and 0 0 2 reflections and EPMA results. They were dependent on substrate temperature. The relation between lattice parameters and the composition, as determined by the intensity ratio, nearly agrees with that of previously reported bulk $Ni_{1-x}S$. The films were stable at room temperature after 1 year, which contrasts with deterioration of bulk $Ni_{1-x}S$. This paper presents SEM and RHEED assessments of the film's morphology and structure.
© 2005 Elsevier Inc. All rights reserved.

Keywords: Nickel sulfide; NiAs-type structure; Epitaxial films; X-ray diffraction; Superstructure; Lattice parameters; Composition; Stabilized films; Morphology; RHEED

1. Introduction

Among nickel sulfides, rhombohedral NiS (millerite) and cubic Ni_3S_4 (polydymite) are stable below the respective temperatures of 652 and 629 K [1]. Single phase of Ni_3S_4 is difficult to be prepared by ordinal solid-state reaction because of the extremely slow reaction rate at low temperatures [1]. In contrast, the hexagonal compound $Ni_{1-x}S$ with a metal-deficient NiAs-type structure—the high temperature form of millerite—is unstable at temperatures less than 555 K at $x = 0.07$ and 652 K at $x = 0.00$ [1–3]. However, this compound is quenched readily at high temperatures. Using quenched specimens, extensive studies have been performed at room temperature or below to assess the compound's physical properties, which are associated with its metal–insulator transition, [4–6]. The specimens deteriorate after several months.

The phase stability ranges of $Ni_{1-x}S$ are $0.0 \leqslant x \leqslant 0.08$ at 800 K and $0.04 \leqslant x \leqslant 0.07$ at 600 K [2]. Generally, metal vacancy takes an ordered arrangement in the NiAs-type structure for transition metal sulfides. That arrangement is alternate stacking of metal-full and metal-deficient layers along the *c*-axis. Consequently, the X-ray reflection condition for $P63/mmc$ of the NiAs-type structure (l =even for 0 0 l) is broken and the reflection 0 0 1 of the structure should appear. An X-ray diffraction study of $Ni_{17}S_{18}$ using single crystals [7] revealed a vacancy-ordered superstructure of the NiAs-type structure as 3a–3b–3c. Electron diffraction studies of $Ni_{1-x}S$ have shown other superstructures [8,9]. Those electron diffraction studies found three coexisting structures in $Ni_{1-x}S$ specimens, indicating that quenched $Ni_{1-x}S$ samples might not have microscopic equilibrium. The superstructures' X-ray reflections are only faintly detectable or are not detectable in reflection data of JCPDS-ICDD, except in those of file no. 76-2306 based on Ref. [7].

Other studies have prepared $Ni_{1-x}S$ films [10,11], but epitaxial films of the compound have not been reported.

*Corresponding author. Fax: +81 29 852 7449.
E-mail address: nozaki.hiroshi@nims.go.jp (H. Nozaki).

0022-4596/$ - see front matter © 2005 Elsevier Inc. All rights reserved.
doi:10.1016/j.jssc.2005.04.009

We unexpectedly obtained an epitaxial $Ni_{1-x}S$ film on MgO(001) in a trial preparation of Ni_3S_4 film at a lower temperature than 555 K. Successive preparation of $Ni_{1-x}S$ films revealed that the film compound was stable for long periods of a year or more at room temperature. The films showed the 0 0 1 superstructure reflection clearly, suggesting a vacancy-ordered arrangement of alternate metal-full and metal-deficient layers along the *c*-axis. The film's crystal structure changes from a hexagonal to a trigonal structure. These film characteristics differed greatly from those of quenched bulk materials of $Ni_{1-x}S$. Furthermore, these trigonal films were arranged epitaxially on cubic substrates of MgO(001). This complex arrangement is a structure in which the film's trigonal axis is parallel to the four-fold rotation axis of the MgO substrate. This paper presents and explains these results.

2. Experimental

Nickel sulfide films were prepared using molecular beam epitaxy (MBE). Previous studies have described the experimental setup [12,13]. Ni powder (5 N sponge powder, Soekawa Chemicals Co. Ltd.) was reduced at 1340 °C under H_2 atmosphere in an MBE chamber until the chamber's oxygen content decreased to the background level. Polished MgO substrates were annealed at 1080 °C in an O_2 atmosphere for 2 h before film growth experiments. Nickel and sulfur molecules were reacted on the substrate under the intensity ratio of the molecular beams, I(S-beam)/I(Ni-beam) = 10. In this experiment, four samples (Film1-Film4) were grown at various substrate temperatures; they are listed in Table 1.

The films' crystallography and epitaxial orientation were determined using an X-ray diffractometer with a convergent X-ray beam with Cu*K*α as described in previous studies; data collection was undertaken similarly [12,13].

Compositional analyses of the films were performed using an electron probe microanalyzer (EPMA, JXA-8500; JEOL). Scanning electron microscope (SEM) images were taken using that device. Film thickness was determined from a cross-section SEM image. Reflection high-energy electron diffraction (RHEED) patterns of the films were obtained using a RHEED gun (VE-052S; Vieetech Japan Co. Ltd.).

3. Results and discussion

3.1. Characterization by X-ray diffraction

First, Film2 was grown at the substrate temperature of 513 ± 6 K. Under this condition, a Ni_3S_4 film was formed on a glass substrate. The resultant material was an epitaxial film of $Ni_{1-x}S$ with a NiAs-type structure. It had a trace amount of Ni_3S_4 with [111] orientation parallel to [001] of the MgO substrate. The resultant material (Film1) was identical to that mentioned above when the substrate temperature was decreased about 10 °C on deposition, but reflections of *lll* ($l = 1-4$) for Ni_3S_4 appeared more clearly.

Typical $\theta - 2\theta$ scanning X-ray diffraction (XRD) patterns of Film2 and Film4 are shown, respectively, in Figs. 1a and 1b, clearly showing reflections of 0 0 1, 0 0 2 and 0 0 4. A very weak reflection 4 4 4 for a foreign phase Ni_3S_4 in Fig. 1a and very weak reflections of 3 0 0 and 6 0 0 for the rhombohedral NiS in Fig. 1b were also detected. X-ray patterns of films (Film1–Film3) prepared using substrate temperatures between 504 ± 6 K and 538 ± 10 K are fundamentally identical to that in Fig. 1a, except that the Ni_3S_4 foreign phase in Film1 and Film2 is replaced by a trace amount of the rhombohedral NiS in Film3. The superstructure reflection of 0 0 1 was clearly visible in the three films' patterns. On the other hand, Fig. 1b shows that the 0 0 1 reflection in the $\theta - 2\theta$ scanning X-ray pattern for Film4 is very weak. Film4 was prepared at the higher substrate temperature of 607 ± 8 K.

X-ray diffraction measurements showed reflection data for lattice planes inclined to (001), which was parallel to the substrate surface. The Bragg condition for each reflection was satisfied by setting the film at appropriate angles of ϕ and Ω rotations for the indicated lattice plane. ϕ is an azimuth within the substrate surface; Ω is an angle around the θ-axis. Observable reflections under the present experimental setup are reflections with $\theta_B > \alpha$, where θ_B is the Bragg angle and α is an interplanar angle between (001) and the indicated lattice plane. This restricted condition results from the fact that the substrate body intercepts reflections with $\theta_B \leqslant \alpha$.

Table 2 lists the X-ray reflections observed for Film2 and Film4. Data at the upper and lower positions in each column, respectively, indicate those for Film2 and

Table 1
Lattice parameters, intensity ratios of 0 0 1 with 0 0 2, compositions, substrate temperatures, and film thickness for $Ni_{1-x}S$ films

Films	*a* (nm)	*c* (nm)	I_{001}/I_{002} (%)	$1-x$ (XRD)	$1-x$ (EPMA)	Substrate temperature (K)	Thickness (nm)
Film1	0.3423(2)	0.5333(3)	17 ± 1.3	0.930 ± 0.003	0.95	504 ± 6	200–220
Film2	0.3421(1)	0.5334(2)	17 ± 1.3	0.930 ± 0.003	0.95	513 ± 6	310
Film3	0.3433(2)	0.5311(3)	16 ± 1.3	0.931 ± 0.002	0.94	538 ± 10	200
Film4	0.3428(2)	0.5339(3)	0.2 ± 0.08	0.993 ± 0.006	0.99	607 ± 8	220

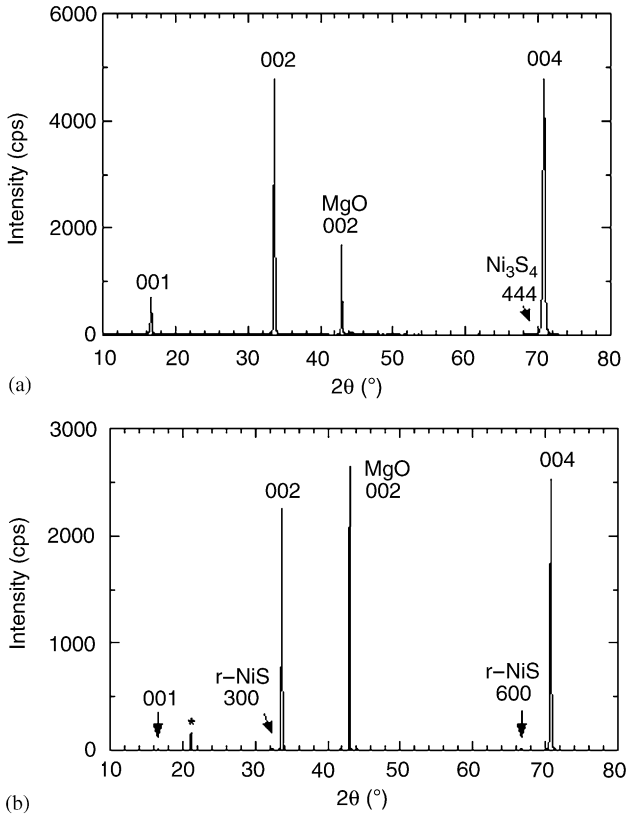

Fig. 1. X-ray diffraction patterns of $Ni_{1-x}S$ films with $\theta - 2\theta$ scanning mode: (a) XRD pattern of Film2, and (b) that of Film4. In Fig. 1b, "r-NiS" represents rhombohedral NiS and reflection marked by * is 0 0 2 of MgO with $\lambda/2$ of Cu$K\alpha$.

Film4. The 0 0 1 reflection is prohibited structurally by $P6_3/mmc$. The films' lattice parameters were obtained using the least-squares method with d-spacing data listed in Table 2. Lattice parameters of the other films were obtained similarly; they are also listed in Table 1.

3.2. In-plane alignment

Results of Figs. 1a and 1b show that (001) of $Ni_{1-x}S$ films are parallel to (001) of MgO substrates. Fig. 2 shows the ϕ-dependence of 1 0 4 reflection intensity for Film2. It was measured to determine the film's in-plane alignment. The lattice plane (104) intersects (001) with a line parallel to the **b**-axis. Therefore, the dependence of 1 0 4 intensity on ϕ-rotation indicates the direction of the **b**-axis within (001). Fig. 2 also shows ϕ-dependence of 1 1 3 reflection intensity for the MgO substrate. The peak position in the ϕ-dependence of 1 1 3 indicates the direction of [110]MgO within (001)MgO. Peak positions of the ϕ-dependence for the 1 0 4 reflection are at every 30°, that is, at 15°, 45° and 75°, etc. This fact arises from in-plane arrangement of sulfur ions on the MgO substrate, as shown in Fig. 3, if a sulfur layer of (001) is adjacent to the substrate surface. In the figure, a two-

Table 2
Observed and calculated d-spacing and observed intensities

hkl	d_{obs} (nm)	d_{cal} (nm)	I_{obs} (%)
0 0 1	0.53348	0.53340	10.3
	0.53393	0.53390	0.1
0 0 2	0.26677	0.26670	60.3
	0.26702	0.26695	66.6
0 0 4	0.13339	0.13335	100.0
	0.13350	0.13348	100.0
1 0 4	0.12163	0.12160	3.1
	0.12180	0.12174	3.9
1 1 4	0.10515	0.10517	15.9
	0.10538	0.10531	16.5
1 0 5	0.10030	0.10037	2.0
	0.10045	0.10048	1.9
2 0 4	0.099113	0.099108	1.2
	0.099310	0.099250	1.5
2 0 5	0.086543	0.86568	2.1
	0.086629	0.086682	1.4
2 1 4	0.085750	0.085754	0.8
	0.085919	0.085890	0.9
1 0 6	0.085120	0.085149	6.2
	0.085132	0.085237	6.5
3 0 4	0.079337	0.079362	18.1
	0.079428	0.079493	6.8
3 1 2	0.078583	0.078527	—
	0.078687	0.078689	11.4

Data at upper and lower positions in each column are for Film2 and Film4, respectively.

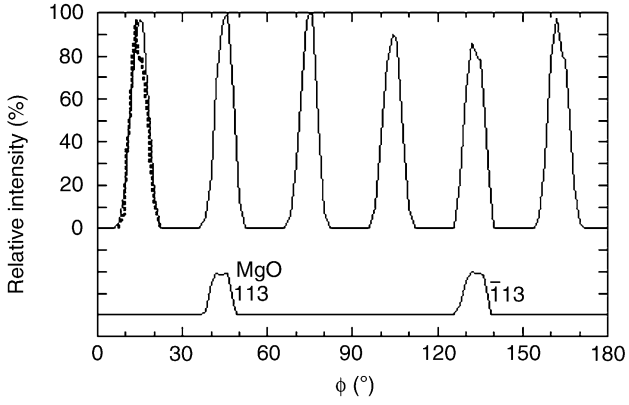

Fig. 2. ϕ-dependence of 1 0 4 intensity of Film2 together with that of 1 1 3 intensity of the MgO substrate. The dotted profile indicates data measured about 1 year later.

dimensional *fcc*-cubic lattice of substrate consists of Mg and O ions, shown as solid and dotted circles. Both two-dimensional hexagonal lattices of sulfur, shown by larger open circles, are depicted as solid and dotted rhombs. The vector $\mathbf{a}-\mathbf{b}$ for the solid rhomb is parallel to $\mathbf{A}+\mathbf{B}$ for MgO; that for the dotted rhomb is parallel to $-\mathbf{A}+\mathbf{B}$. In addition, Fig. 2 shows the in-plane arrangement, coexistence of the trigonal axis for the $Ni_{1-x}S$ lattice, and the four-fold rotation axis of

[001]MgO. Those axes are mutually parallel, giving the appearance of twelve-fold rotational symmetry in the ϕ-dependence of 1 0 4 reflection intensity.

Length $|\mathbf{a}-\mathbf{b}|$ is 0.5925–0.5946 nm for Film1–Film4. Fig. 3 shows that the magnitude agrees well with the diagonal length of $|\mathbf{A}+\mathbf{B}|$ (0.5958 nm) within 0.6% length mismatch at most. On the other hand, sulfur arrays along $\mathbf{a}+\mathbf{b}$ for the solid rhomb, that is, the direction perpendicular to $\mathbf{a}-\mathbf{b}$, overlap the Mg arrays of the substrate along the same direction. The relation between the S–S distance, $|\mathbf{a}+\mathbf{b}|$, and Mg–Mg distance, $|\mathbf{B}-\mathbf{A}|/2$, along this direction is $7|\mathbf{a}+\mathbf{b}| = 4|\mathbf{B}-\mathbf{A}|$, suggesting a 0.8% mismatch at most. The situation for the dotted rhomb is the same as that for the solid rhomb. We therefore infer that these conditions engender epitaxy of a $Ni_{1-x}S$ hexagonal lattice on the cubic MgO substrate, as observed.

Table 3 shows that the integral breadth of the Ω rocking profile (θ scanning profile) for X-ray reflection decreases with increasing the substrate temperature. The lattice plane of (304) shown in the table is at the largest angle of 53.4° with (001) for the lattice planes listed in Table 2. Therefore, the integral breadth of (304) reflects incompleteness of in-plane alignment, whereas the integral breadth of (002) reflects the incompleteness of out-of-plane epitaxy. For that reason, completeness of out-of-plane epitaxy and in-plane alignment increases with increasing substrate temperature.

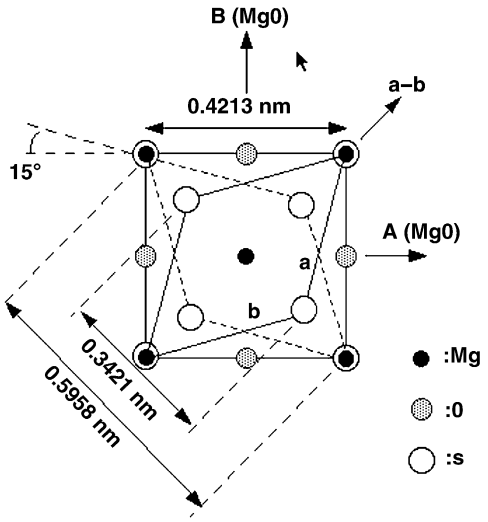

Fig. 3. Schematic illustration of in-plane epitaxial relations between two-dimensional hexagonal lattices of $Ni_{1-x}S$ film and the two-dimensional face-centered cubic lattice of MgO(001) substrate. Open circles in solid and dotted rhombs represent S ions. Solid and dotted circles, respectively, represent Mg and O ions.

Table 3
Integral breadth of Ω rocking profile

hkl	$\Delta\Omega$ (Film1) (°)	$\Delta\Omega$ (Film2) (°)	$\Delta\Omega$ (Film3) (°)	$\Delta\Omega$ (Film4) (°)
0 0 2	1.47	1.10	0.277	0.239
3 0 4	1.21	0.894	0.273	0.186

3.3. Film composition

It is noteworthy that the existence of 0 0 1 indicates an ordered arrangement of metal vacancies in alternate metal layers along the c-axis. The intensity ratio between 0 0 1 and 0 0 2 reflections is dependent on the magnitude of $1-x$ in $Ni_{1-x}S$ and on the degree of metal-vacancy ordering between both metal-deficient and metal-rich layers. Table 1 lists the films' compositions, as estimated by the intensity ratio between 0 0 1 and 0 0 2 and those by EPMA. The magnitude of $1-x$ for XRD indicates a perfect metal-vacancy ordering in which fully occupied metal layers and metal-deficient layers are stacked alternately.

Both XRD and EPMA results showed that the magnitude of $1-x$ increased with increasing substrate temperature. This result is reasonable because sulfur concentration on the substrate surface decreases upon deposition with increasing substrate temperature. The magnitude $1-x$ for XRD is systematically smaller than that for EPMA except for the case of Film4. The EPMA data were collected using characteristic X-rays of Ni$L\alpha$ ($\lambda = 1.4595$ nm) and S$K\alpha$ ($\lambda = 0.5373$ nm) under an acceleration voltage of 5 keV to avoid undesirable X-ray generation from the substrate. Considering that the long wavelength of Ni$L\alpha$ requires a large absorption correction to determine the composition of the film, the EPMA results agree well with the XRD results. Partial disordering of metal vacancy between both metal-rich layers and metal-deficient layers gives a smaller value of $1-x$ for XRD than that the perfect ordering does. Therefore, the assumption of alternating fully occupied metal layers and metal-deficient layers is adequate for the EPMA results of Film1–Film3.

The composition dependences of lattice parameters of bulk $Ni_{1-x}S$ are shown in Fig. 4 [7,14,15]. Open circles in that figure show lattice parameters of the present films with compositions estimated by XRD. The data of Film1–Film3, except for the c dimension of Film3, agree well with lines fitting data of bulk $Ni_{1-x}S$ by the least-squares method. This agreement suggests that the perfect ordering of metal vacancies pertains for Film1–Film3. However, the lattice parameters of Film4 are rather smaller than those of bulk $Ni_{1-x}S$. The composition of Film4, as determined by XRD, agrees well with that done by EPMA. However, the actual composition $1-x$ of Film4 might be smaller than the composition determined by XRD because it moves the open circles of Film4 nearer the line of bulk $Ni_{1-x}S$ in Fig. 4. For this case, partial disordering of metal vacancy may occur in contrast with the cases of Film1–Film3. The metal–insulator transition temperature of Film4 given by a

resistivity measurement will give other information because the transition temperature should depend strongly on composition.

3.4. SEM images

SEM images of Film2, Film3 and Film4 are presented, respectively, in Figs. 5a–c in the order of increasing substrate temperature of the film. The image of Fig. 5a shows aggregation of polyhedral grains, whereas that of Fig. 5c shows jigsaw-puzzle-like grains on the film surface. The latter is considered to result from coalescence of polyhedral grains with the same in-plane orientation. The image of Fig. 5b might show an intermediate stage of coalescence from aggregation of polyhedral grains in the image of Fig. 5a to grains like the jigsaw puzzle in Fig. 5c. Thereby, the films' morphology appears to change systematically with increasing substrate temperature.

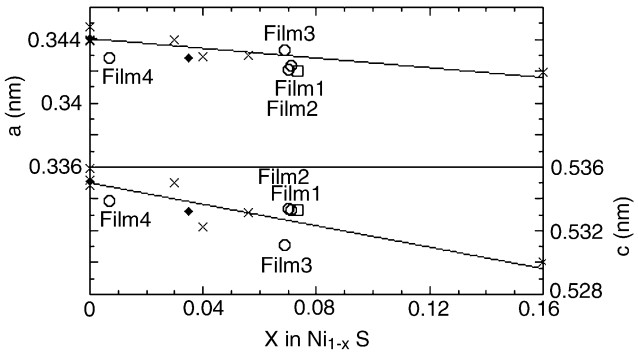

Fig. 4. Composition dependence of lattice parameters. Open circles represent data of the present films just after their preparation. Open squares indicate results for Film2 after about 1 year. Solid circles and crosses are data of bulk $Ni_{1-x}S$ [7,14,15].

3.5. RHEED patterns

A RHEED pattern of Film3 measured immediately after film preparation is shown in Fig. 6a. The incident electron beam was set along the direction at an azimuth of 15° with [100]MgO. Distances of streaks (D) in the pattern are incommensurate; $D(a,b) = D(b,d) = D(a,c)/\sqrt{3}$. The two-domain structure revealed by the XRD experiment is shown in Fig. 7. That figure depicts the two-dimensional reciprocal lattice of the film. It includes both hexagonal lattice domains, which mutually overlap with 30° rotation. Along the direction perpendicular to the incident electron beam, **a***, of one

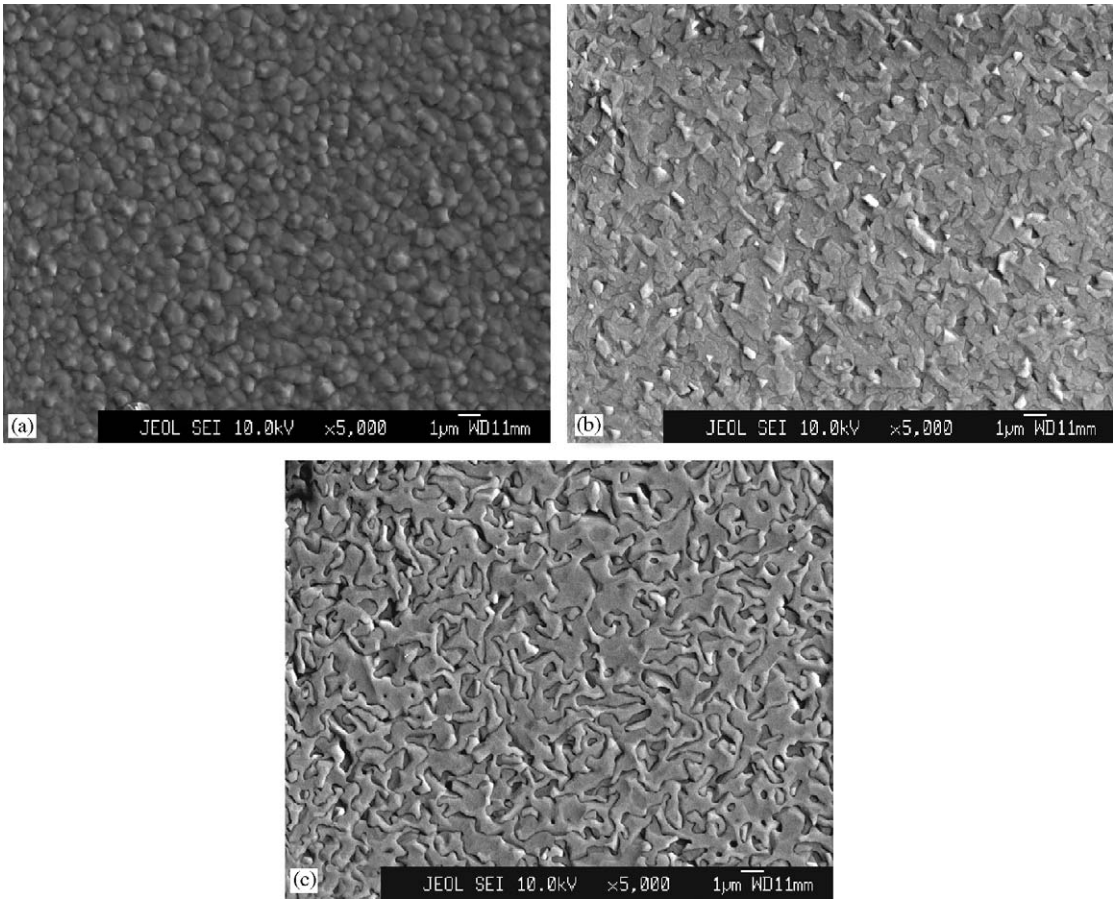

Fig. 5. SEM images of $Ni_{1-x}S$ film: (a) Film2, (b) Film3 and (c) Film4.

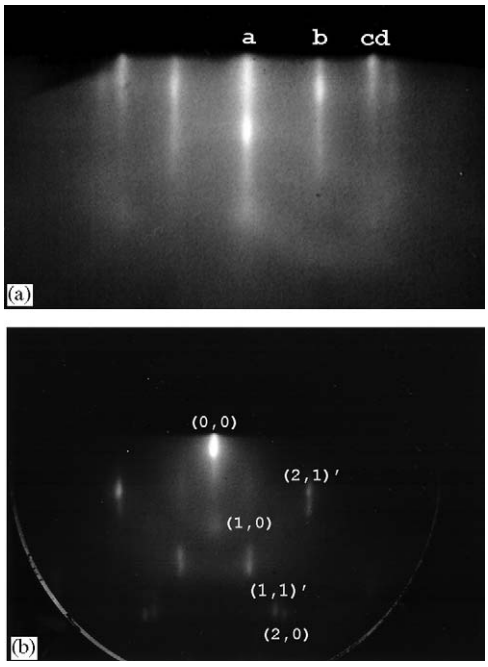

Fig. 6. RHEED patterns: (a) with incident electron beam along the direction at an azimuth of 15° with [100]MgO for Film3 and (b) with that along direction parallel to [100]MgO for Film2. In (a), distance ratios between the streaks are $D(a-b) : D(a-c) : D(a-d) = 1 : \sqrt{3} : 2$.

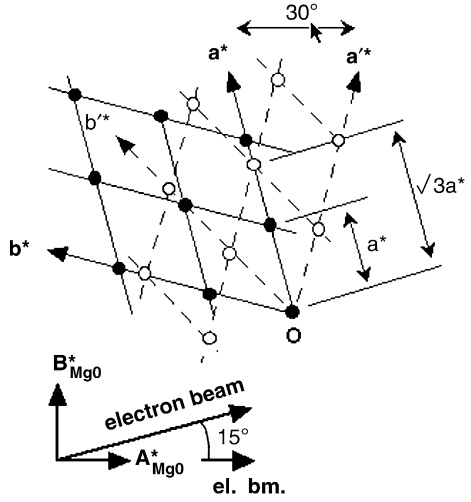

Fig. 7. Schematic illustration of two-dimensional reciprocal lattice of $Ni_{1-x}S$ film. It includes two lattice domains generated by 30° rotation to each other. Directions of the incident electron beam are perpendicular to $\mathbf{a}^*$ for the case of Fig. 6a, and parallel to $\mathbf{A}^*_{MgO}$ for the case of Fig. 6b.

hexagonal lattice domain overlaps with $\mathbf{a}^{*\prime}+\mathbf{b}^{*\prime}$ of another, thereby giving an incommensurate pattern of the 0th Laue zone.

RHEED experiments for Film2 and Film4 were not made immediately after their preparation. However, RHEED experiments for Film2, Film3 and Film4 were performed after a 10–12 month period. The specimens were exposed to air during about 1 month during performance of other experiments; subsequently, they were stored in vacuum. A RHEED pattern of Film3 measured after a 10-month period was identical to that observed initially, but its reflection was rather weak. Similar patterns for Film2 and Film4 were unobtainable because of very weak reflections. However, a RHEED pattern for Film2, as shown in Fig. 6b, was obtained with the incident plane of the electron beam parallel to (010)MgO after about 1 year. Reflections shown on the right side were indexed using the reciprocal lattice of Fig. 7. Reflections on the left side were explainable using another reciprocal lattice caused by the mirror plane of (010)MgO. RHEED patterns of Film3 and Film4 resemble those of Fig. 6b. They were obtained after a 10-month period. Therefore, RHEED results indicate that atom arrangements in the film surfaces are identical to those for the inner volume of the film obtained using X-ray diffraction.

3.6. Film stability

Stability of Film2 was confirmed by reinvestigating the $\theta-2\theta$ scanning XRD pattern about 1 year later. The XRD pattern was almost unchanged in comparison with the result of Fig. 1a. However, the intensity ratio between 0 0 1 and 0 0 2 reflections increased slightly from $17\pm1.3\%$ for fresh Film2 to $19\pm1.5\%$ for the film after about 1 year. The latter value indicated a magnitude of $1-x=0.927\pm0.03$: the Film2 composition about 1 year later was slightly more metal-deficient than fresh Film2. Furthermore, trace reflections for 1 1 1 of Ni_3S_4 and 1 0 1 and 3 0 0 of rhombohedral NiS appeared in the pattern together with 4 4 4 of Ni_3S_4 that was observed previously for the fresh film.

Lattice parameters of Film2 were reexamined about 1 year after preparation of Film2. Results were $a=0.3420(3)$ nm and $c=0.5333(5)$ nm, which were slightly smaller than the previous results of $a=0.3421(1)$ nm and $c=0.5334(2)$ nm. However, they are consistent with the increased intensity ratio between 0 0 1 and 0 0 2 reflections and the occurrence of rhombohedral NiS for Film2 after about 1 year. Although the extremely small decrease of the lattice parameters and the small increase of the intensity ratios seemed to be within experimental error, it was difficult to rule out the possibility that a minor change in composition for Film2 might occur, thereby causing rhombohedral NiS segregation. However, the SEM image of Fig. 5a, which was measured 9 months after its preparation, appeared to give no clear evidence of the segregation. For that reason, we infer that the slight occurrence of rhombohedral NiS results from crystallization of an amorphous-like phase coexisting on the preparation of Film2. The relation between composition and lattice parameters for Film2 about 1

year later is shown by open squares in Fig. 4. Results of Fig. 4 indicate that changes in lattice parameters and composition of Film2 after 1 year are very slight, even if they occur.

The ϕ-dependence of 1 0 4 reflection intensity for Film2 was also unchanged within experimental accuracy, as indicated by the dotted profile in Fig. 2, which depicts a reinvestigated result about 1 year later. Furthermore, appearances of the optically reflecting films had not changed. Therefore, these films deposited on MgO substrates are stable as implied by the minor changes in the crystal structures of Film2 and by the lack of change in their optical reflectance.

4. Conclusions

Epitaxial $Ni_{1-x}S$ films with NiAs-type structure were prepared on MgO(001) substrates using MBE. The films were characterized using X-ray diffraction. Epitaxial film orientations were (001)[1,−1,0]$Ni_{1-x}S$||(001)[110]MgO and its equivalents, which resulted from coexistence of the trigonal axis of the film and the four-fold rotation axis of the substrate. RHEED patterns of the film agree with the orientations obtained by XRD.

Observation of 0 0 1 reflections indicated that nickel vacancies were arranged in an ordered fashion along the *c*-axis. The 0 0 1 intensity was dependent on the substrate temperature of the film. The intensity ratio between 0 0 1 and 0 0 2 reflections indicated the films' composition. The relation between lattice parameters of the films and their compositions almost agrees with that of previously reported bulk $Ni_{1-x}S$.

Film stability was examined using XRD after 1 year. The lattice parameters, the epitaxial orientations, and the intensity ratio between 0 0 1 and 0 0 2 were all unchanged within experimental accuracy. RHEED patterns were also fundamentally unchanged. For those reasons, the films were inferred to be stable at room temperature, in contrast with $Ni_{1-x}S$ bulk materials. Surface morphology of each film, as observed using SEM, was dependent on the substrate temperature.

Acknowledgments

The authors are grateful to Dr. M. Onoda for discussion of crystallography, and to Ms H. Aoki for SEM image collection.

References

[1] G. Kullerud, R.A. Yund, J. Petrol. 3 (1962) 126–175.
[2] F. Grønvold, S. Stølen, Thermochim. Acta 266 (1995) 213–229.
[3] H. Rau, J. Phys. Chem. Solids 36 (1975) 1199–1204.
[4] J.T. Sparks, T. Komoto, Phys. Lett. 25A (1967) 398–399.
[5] S. Anzai, M. Matoba, M. Hatori, H. Sakamoto, J. Phys. Soc. Jpn. 55 (1986) 2531–2534.
[6] D.D. Sarma, S.R. Krishnakumar, N. Chandrasekharan, E. Weschke, C. Schüßler-Langeheine, L. Killan, G. Kaindl, Phys. Rev. Lett. 80 (1998) 1284–1287.
[7] G. Collins, C. Chavant, R. Comès, Acta Cryst. B 39 (1983) 289–296.
[8] S.N. Black, D.A. Jefferson, P. Henderson, J. Solid State Chem. 53 (1984) 76–86.
[9] C.h.B. Lioutas, C. Manolikas, G. Van Tendeloo, J. Van Landuyt, J. Cryst. Growth 126 (1993) 457–465.
[10] S.D. Sartale, C.D. Lokhande, Mater. Chem. Phys. 72 (2001) 101–104.
[11] H. Lee, M. Kanai, T. Kawai, S. Kawai, Jpn. J. Appl. Phys. 32 (1993) 2100–2101.
[12] H. Nozaki, M. Onoda, K. Kurashima, T. Yao, J. Solid State Chem. 157 (2001) 86–93.
[13] H. Nozaki, M. Onoda, K. Yukino, K. Kurashima, K. Kosuda, H. Maki, S. Hishita, J. Solid State Chem. 177 (2004) 1165–1172.
[14] J.M.D. Coey, R. Brusetti, A. Kallel, J. Schweizer, H. Fuess, Phys. Rev. Lett. 32 (1974) 1257–1260.
[15] JCPDS–International Center for Diffraction Data, Nos. 02-1273, 02-1277, 50-1791, 65-0395, 65-5762, and 89-7141.